# Chapter 3

# Blume-Capel ($S = 1$) ferromagnet driven by propagating and standing magnetic wave.

## 3.1 Introduction:

In the previous chapter, I mainly discussed nonequilibrium phase transition in Ising ($S = \frac{1}{2}$) ferromagnet. Systems having anisotropy, such as crystal field anisotropy, may also be studied under nonequilibrium conditions. Blume-Capel(BC) ferromagnet is one such anisotropic system. BC model [[1]-[15],[16]-[19]] has long been used to study various kind of systems having spin anisotropy such as $Al-Fe$ alloy etc. Application of perturbation to such systems by externally applied spatio-temporally varying field affects the dynamic nature of such system. In the following section I will discuss the effect of propagating magnetic wave and standing magnetic wave on BC($S = 1$) ferromagnet. The reference of the journal, in which this work (research article) was published is given here:
**Muktish Acharyya** and **Ajay Halder** *J.Magn.Magn.Mater.* **426**(2017)53

## 3.2 Magnetic waves through BC ferromagnet:

When a magnetic wave passes through a BC ferromagnet the spins of the system feel different kind of magnetic perturbation at any instant, the value and nature is determined by the form of the magnetic wave that perturbs the system. The important aspect of BC ferromagnet is that the spins prefer some orientations, due to the anisotropy, to other orientations. The perturbing field tries to orient the spins towards its direction, thus competes with the intrinsic anisotropy of the system. Depending on the temperature, the strength of the magnetic perturbation and the strength of anisotropy different kind of dynamical phases are formed with their characteristic behaviors, which are the main objectives of study in this section.

### 3.2.1 Response to propagating magnetic wave:

The time dependent Hamiltonian of the two-dimensional Blume-Capel ferromagnet (having uniform nearest neighbor interaction) in presence of a magnetic field wave (having spatio-temporal variation) can be expressed as [4]-

$$H(t) = -J\Sigma\Sigma' s^z(x,y,t)s^z(x',y',t) + D\Sigma(s^z(x,y,t))^2 - \Sigma h^z(x,y,t)s^z(x,y,t), \quad (3.1)$$

where, $s^z(x,y,t)$ represents the $z$ component of the spin ($S = 1$). $s^z$ takes any of the three values of spin state, viz, $+1,\ 0\ or\ -1$, for ($S = 1$). The first and the third

terms represent respectively the spin-spin cooperative energy and the spin-magnetic field interaction energy. The magnetic field $h^z(x, y, t)$ at site $(x, y)$ at time $t$, has the following form of propagating wave:

$$h^z(x, y, t) = h_0 cos(2\pi ft - 2\pi\frac{y}{\lambda}).$$

Here, $h_0, f$ and $\lambda$ represent respectively *the field amplitude, the frequency of magnetic field oscillation and the wavelength* of the propagating magnetic wave.The cooperative ferromagnetic interaction strength, $J(> 0)$, is considered to be uniform throughout the system. The positive second term represents the spin anisotropy within the system, where $D$ is the strength of the anisotropy. The energy at the spin sites having spin values ($s^z = \pm 1$) is larger relative to the sites with spin value ($s^z = 0$). Manifestation of spin anisotropy occurs in the relative distribution of the three spin states. Depending on the values of the strength of anisotropy, magnetic field strength, strength of ferromagnetic interaction and temperature the *relative* population of the spin states in the BC ferromagnet vary.

**Monte-Carlo simulation:**

As discussed in our earlier studies, here also a square lattice of dimension $L \times L$ is considered over which the spins are arranged. The dynamics of such spins are generated by *Monte-Carlo* method. We consider only the bulk behavior of a $2D$ BC ferromagnet; so, to preserve the translational invariance periodic boundary conditions are applied in both the $x$ and $y$ directions of the square lattice. The initial configuration of spins in the lattice corresponds to the high temperature random phase where the three values of spin states $(+1,\ 0,\ -1)$ are uniformly distributed (with equal probability) over all the lattice sites. This is the high temperature paramagnetic configuration of the system. At any temperature, the BC ferromagnetic spins respond to magnetic perturbation, in the form of propagating wave and show its dynamical behavior. These responses depend on the values of the parameters such as cooperative interaction strength, the strength of anisotropy and the instantaneous value of the magnetic field. Every dynamical steady state is reached by cooling the system slowly i.e. by decreasing the temperature in small values. Steady state behavior at any particular temperature is observed by keeping the BC ferromagnet at that particular thermal bath for a sufficiently long time. During this

time the spins are updated, using parallel updating rule, according to the Metropolis rate given by *equation 2.3* :

$$W(s_i^z \rightarrow s_f^z) = Min[exp(-\Delta E/kT), 1].$$

Here $s_i^z$ and $s_f^z$ represent the initial and final values of any spin state at a site $(x, y)$, before and after updating, respectively. $\Delta E$ represents the change in energy due to spin flip from initial state to final state; $k$ is the Boltzmann constant. During updating of spins every site of lattice, having initial spin state $s_i^z$, is taken one by one. Then, any spin value ($s^z = 0, \ +1 \ or \ -1$) is chosen at random with a probability $\frac{1}{3}$. We call it the final spin state $s_f^z$. Next, calculating the change in energy $\Delta E$ due to the spin flip, the spin value at the site is now updated to this final value from its initial value with the Metropolis probability as written above. The field amplitude $h_0$, and the strength of anisotropy $D$ are measured in the unit of $J$ and the temperature $T$ is measured in the unit of $\frac{J}{k}$. The unit of time is the standard Monte-Carlo time *MCSS*, defined as the time required to update an $L^2$ number of spins once in an $L \times L$ square lattice.

**Results:**

Using the above described MC technique the dynamical evolution of a BC ferromagnet under the influence of propagating magnetic field wave have been simulated. As the BC ferromagnet is cooled below a certain temperature, called the dynamical transition temperature $T_d$, it undergoes phase transition from high temperature paramagnetic phase to the low temperature pinned phase. The paramagnetic phase is the symmetric phase, having no net magnetization. In the high temperature, alternate bands of spins having spin values $s^z = +1$ and $s^z = -1$ are formed which propagates coherently along the direction of the propagating wave. A few sites having spin values $s^z = 0$ are found along the boundaries of the bands. *Figure 3.1* shows the coherent propagation of spin-waves. Here the lattice size is $L = 100$ lattice units (lu). The driving propagating magnetic wave has wavelength $\lambda = 50$ lu and frequency $f = 0.01 \ MCSS^{-1}$. At higher temperature thermal fluctuations of spins are quite high and the externally applied magnetic field orients the spins along its direction. At the boundaries of the spin bands, where strength of the magnetic field is nearly zero, the population of spin states $s^z = 0$ increases. This population depends on the value of the strength of anisotropy $D$. It may

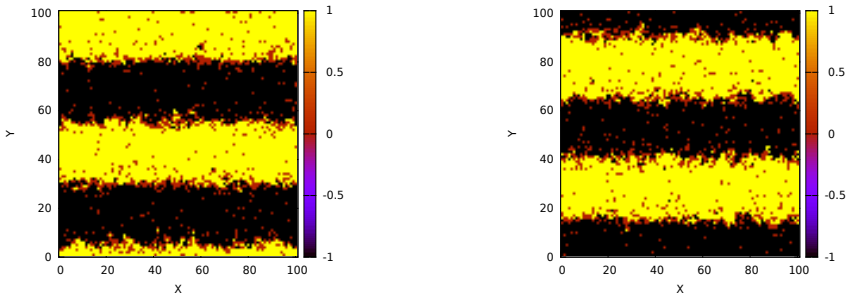


Figure 3.1: (Color online) Coherent propagation of driven spin-wave shown here for two different values of time. **Left** is for $t = 2000$ and **right** is for $t = 2070$. Here $D = 1.0,\ H(or\ h_0) = 1.5,\ T = 1.0$.

be noted here that the conventional notion of spin-wave excitation in condensed matter physics has nothing to deal with the term *spin-wave* used here.

At lower temperatures coherent propagation of spin-waves is absent. Most of the spins are pinned or frozen to any one value of $s^z = \pm 1$. As the thermal fluctuations get reduced at lower temperatures, the spin-spin ferromagnetic interaction locks the spins to remain parallel and the propagating magnetic field also has minimum effect on the spins of the system. Here the strength of propagating field is incapable of flipping the spins. If the magnetic field amplitude becomes higher, spins will interact strongly with the field and the dynamic transition temperature will reduce further. Thus, two distinct dynamical phases, namely: *spin-wave* propagating phase and *spin-frozen* or pinned phases are observed. The dependence of these dynamical phases on $D$, $h_0$, ($H$ in figure) and $T$ are shown in a comprehensive manner in *figure 3.2*. We have observed [20] similar bands of spins propagating with the propagating wave in a 2D Ising ferromagnet also (see section 2.2.1). However, in the BC ferromagnet, the spin state $s^z = 0$ has lower anisotropy energy relative to the spin states $s^z = \pm 1$. Hence, with the increase in the strength of anisotropy $D$, the relative probability of the states with spin value $s^z = 0$ increases. It is observed that, in the propagating phase, when the field amplitude ($h_0$, ($H$ in figure)) is high and the temperature ($T$) is close to (but above) the transition temperature, the population of $s^z = 0$ has increased near the *interfaces* of alternate spin bands of $s^z = \pm 1$ (see *fig. 3.2(iii)*). This is because the strength of the magnetic field is minimum ($h^z(x, y, t) = 0$) at the interface. Hence, the magnetic field cannot orient the spins along its direction. On the other hand, the anisotropy energy flips the spins more to the $s^z = 0$ state while increasing their relative population.

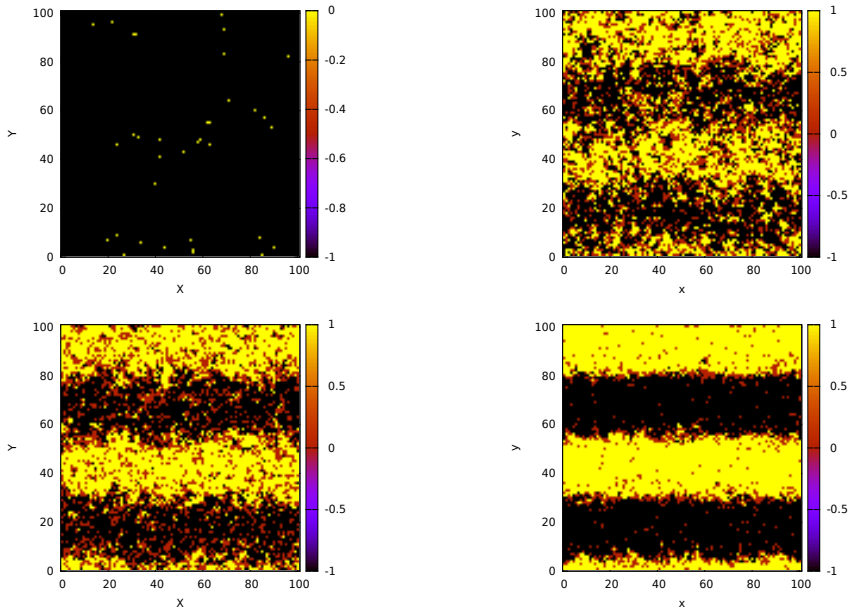


Figure 3.2: (Color online) Morphology of the lattice (value of $S_z(x, y, t = 2000)$) for different values of $T$, $H$ *and* $D$. **Clockwise from top-left (i)** $D = 1.0,\ H = 0.5,\ T = 0.5$**, (ii)** $D = 0.1,\ H = 0.3,\ T = 1.9$**, (iii)** $D = 1.0,\ H = 1.5,\ T = 1.0$**, (iv)** $D = 1.0,\ H = 0.5,\ T = 1.5$**.**

Different steady state dynamical quantities are measured to detect the phase transition. The dynamical order parameter $Q$ for this phase transition is defined as the time averaged magnetization per lattice site over the full cycle of the propagating magnetic wave, which is given as follows:

$$Q = f \oint M(t)\, dt. \tag{3.2}$$

Here, $M(t)$, defined as:

$$M(t) = \frac{1}{L^2} \Sigma_i s_i^z(x, y, t), \tag{3.3}$$

is the instantaneous value of magnetization per site. The summation runs over all the $L^2$ lattice sites. Due to the intrinsic stochasticity in the Metropolis dynamics, the process generates different values of order parameter, $Q$, in different cycles. As a result, $Q$ has a statistical distribution. The variance of $Q$ is defined as $V = L^2(\langle Q^2 \rangle - \langle Q \rangle^2)$, where the symbol $\langle .. \rangle$ denotes average over all the values of the quantities obtained from different cycles in steady state. The dynamic phase transition is studied quantitatively by studying the temperature variation of $Q$ and $V$ with $h_0$, ($H$ in the figures), and $D$ as parameters. These are shown in *figure 3.3*. To obtain the steady state values of $Q$ and $V$ here, the system is allowed to pass through the constant temperature heat bath for $10^5$ $MCSS$,

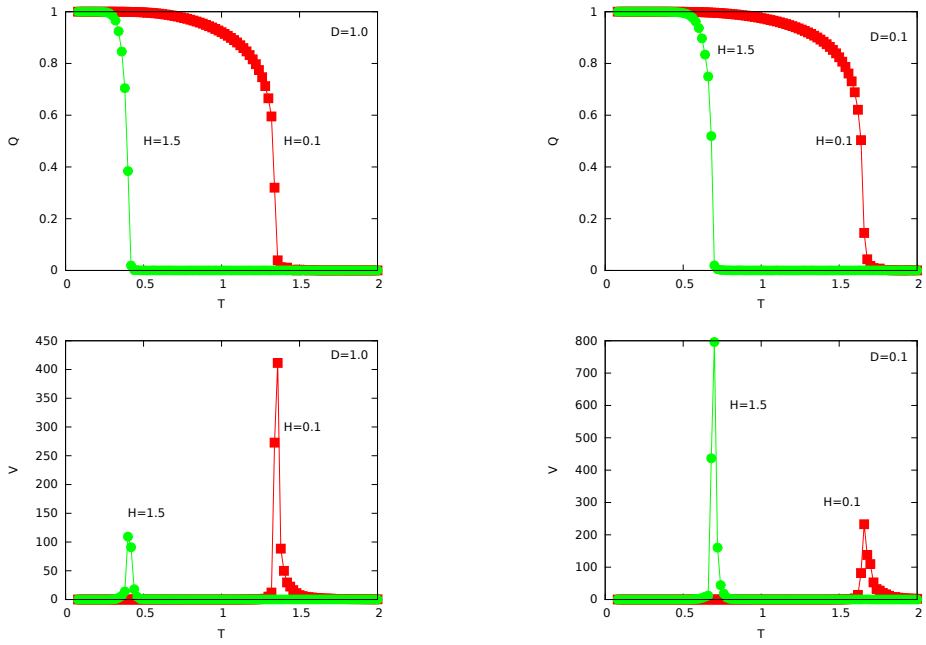


Figure 3.3: Temperature dependence of $Q$ and $V$ for two different values of $H$. Here, $D = 1.0$ (**left**) and $D = 0.1$ (**right**).

while initial (or transient) changes in it for $5 \times 10^4$ $MCSS$ are discarded. It was checked that this length of simulation is sufficient to achieve nonequilibrium steady state. Since $f = 0.01$, 500 cycles of propagating magnetic field are thus considered to measure $Q$ and $V$. It has been checked that this number of cycles is sufficient to have good statistics. The dynamical order parameter $Q$ assumes non-zero values (see $Q-T$ variations in *figure 3.3*) as the system is cooled slowly below certain transition temperature $T_d$ showing the dynamical phase transition. From the temperature dependence of $Q$, the transition seems to be continuous in nature. In this particular example the BC ferromagnet starts cooling at high temperature, 2.00, in small decrement, of 0.02, in temperature. The transition temperature is noted from the sharp peak in the $(V - T)$ variation of variance $(V)$ with respect to temperature $(T)$, which is also shown in the *figure 3.3* above. It is believed to diverge in the limit $L \to \infty$.

The dependence of transition temperature on $h_0$, ($H$ in the figure), is evident in these figures. The transition temperature decreases for higher field amplitudes $h_0$, of the propagating magnetic field, for a fixed value of strength of anisotropy $D$. The result is quite justified; similar to our discussion in results of *section 2.2.2*. Here is a typical example as shown in the figure. When $D = 1.0$, the peaks of $V$ are observed at $T = 0.40$

and $T = 1.36$ for $h_0 = 1.5$ and $h_0 = 0.1$ respectively, whereas for a lower value of anisotropy, $D = 0.1$, the peaks are observed at values $T = 0.70$ and $T = 1.66$ for same set of values of $h_0$ respectively.

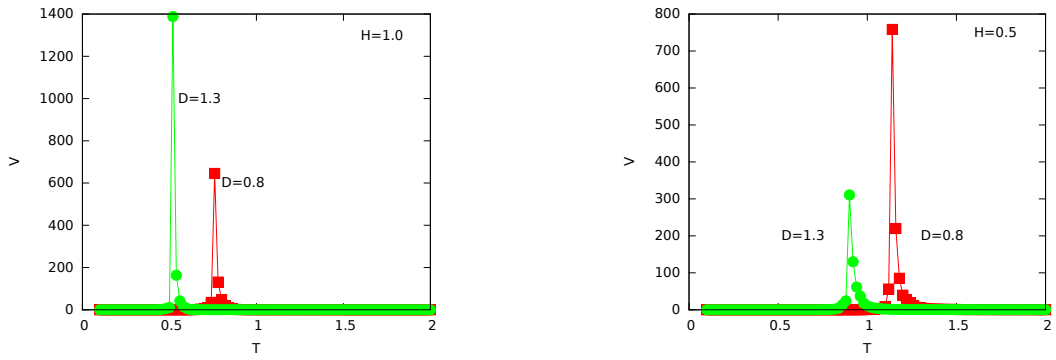


Figure 3.4: Temperature dependence of $V$ for two different field amplitudes $H$ and $D$. $D = 0.8$ (Red square) and $D = 1.3$ (Green bullet).

For a fixed value of $h_0$, the transition occurs at lower temperature as one increases the value of $D$, the strength of anisotropy, showing the dependence of transition temperature on values of $D$ for fixed $h_0$. This result is shown in *figure 3.4*. Here is an example; for $h_0 = 1.0$, transition temperatures are $T = 0.52$ and $T = 0.76$ for $D = 1.3$ and $D = 0.8$ respectively. Similarly, for $h_0 = 0.5$, the transitions occur at $T = 0.90$ and $T = 1.14$ for same set of $D$ respectively.

The dynamical phase boundaries may be obtained in two different planes $(D-T)$ for different values of $h_0$, ($H$ in figure) and $(h_0 - T)$ for different values of $D$. For different set of values of $D$ and $h_0$, the transition temperature is obtained from the peak values of the temperature variation of variance of order parameter $(Q)$. It is seen from the *figure 3.5* that the phase boundaries, in the $(h_0 - T)$ plane, shrink towards the low field and low temperature region for higher values of strength of anisotropy $D$, implying lower transition temperature. Similarly, the dynamical phase boundaries in the $(D-T)$ plane also shrink inwards (low temperature and low $D$) for the higher values of magnetic field amplitude $h_0$. In both the situations the transitions observed, along the entire boundary, are continuous in nature. It may be noted that the equilibrium transition temperature (for $D = 0$ and $h_0 = 0$) is very close to the value 1.8 (see *fig.2 of Ref.[12]*). The results for $D = 0.1$, obtained here, may be compared to this value.

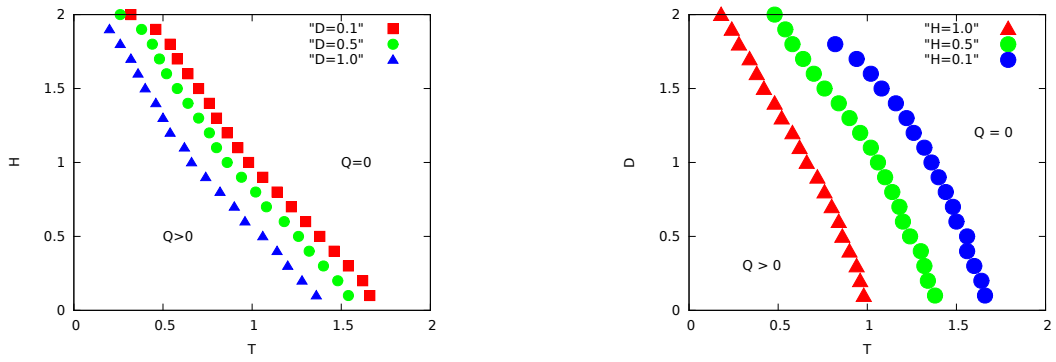


Figure 3.5: Phase diagram in (**Left**) the $H-T$ plane for different values of $D$ (mentioned in the figure) and (**Right**) the $D-T$ plane for different values of $H$ (mentioned in the figure) in the case of propagating wave.

### 3.2.2 Response to standing magnetic wave:

In this subsection, I will now discuss the effect of standing magnetic field wave form of magnetic field on BC($S=1$) ferromagnet. The Hamiltonian for the BC ferromagnet under the influence of standing magnetic wave has the same form as equation 3.1, which may be rewritten here as follows:

$$H(t) = -J\Sigma\Sigma' s^z(x,y,t)s^z(x',y',t) + D\Sigma(s^z(x,y,t))^2 - \Sigma h^z(x,y,t)s^z(x,y,t).$$

The perturbation provided by the magnetic field has the form of standing wave,

$$h^z(x,y,t) = h_0 sin(2\pi ft)sin(2\pi\frac{y}{\lambda}).$$

Here, the parameters used, have their usual meaning as in the previous section. The spatial distribution of the three different spin states ($s^z = 0, \pm 1$) depends on different parameters such as temperature $T$, strength of anisotropy $D$, strength of magnetic field $h_0$ and the mutual cooperative interaction strength $J$.

**Simulation:**

An $L \times L$ square lattice may again be considered here, over which the ferromagnetic spins are arranged. Periodic boundary conditions are applied in both the directions to preserve the translational invariance. The standard *Monte-Carlo* method is used to simulate the dynamics of spins of the BC ferromagnet under the influence of standing magnetic wave. Starting from the high temperature *random* configuration, where all the spins states are

equally probable, the system is cooled down slowly by a small change in temperature in each step to reach any dynamical steady state of the ferromagnet. Using MC technique, the spin dynamics may be viewed and the steady state quantities are calculated. The change in total spin configuration of the ferromagnet is generated at Metropolis rate, given by *equation 2.3*;

$$W(s_i^z \rightarrow s_f^z) = Min[exp(-\Delta E/kT), 1].$$

As usual convention, the field amplitude $h_0$, and the strength of anisotropy $D$ are measured in the unit of $J$ and the temperature $T$ is measured in the unit of $\frac{J}{k}$. The unit of time is the standard Monte-Carlo time steps per site *MCSS*, defined as the $L^2$ number of moves.

**Results:**

Two distinct dynamical modes of ferromagnetic spins are also present here when the system is under the field variation of standing magnetic wave. For a fixed set of values of $h_0$ and $D$, a *spin frozen* state, also called the *pinned* phase, is observed in low temperature. In contrast, at higher temperatures, formation of alternate ($s^z = +1$ & $s^z = -1$) spin bands is observed. The population of spin state $s^z = 0$ is relatively small as compared to the states $s^z = \pm 1$. The spins having value $s^z = 0$ are scattered near the interface of alternate bands of spin-values $s^z = \pm 1$. These spin bands form a *standing spin wave*, which *do not* propagate like the spin-bands in case with propagating magnetic wave. This phase is known as the *standing spin-wave* phase. Precisely speaking, the system undergoes a nonequilibrium phase transition from a standing spin-wave phase to a spin frozen phase as the temperature is lowered. The morphology of spin states in both of these phases are shown in the *figure 3.6*. $H$ in the figures represent the field amplitude $h_0$. We have observed a similar pattern of standing magnetic wave in Ising ferromagnet swept by standing magnetic wave (see *section 2.2.2*). Here a population of spins with $s^z = 0$, is also present near the interface of alternate bands.

The propagating spin-wave phase and the standing spin-wave phases are dynamically different. This is evident from the dynamics of the spin configurations in the lattice. *Figure 3.7* shows the snap shot of lattice spins at two different times at ($t = 1000$ MCSS and $t = 1070$ MCSS) for a fixed set of values of $T$, $D$ and $h_0$ ($H$ in figure). There is no

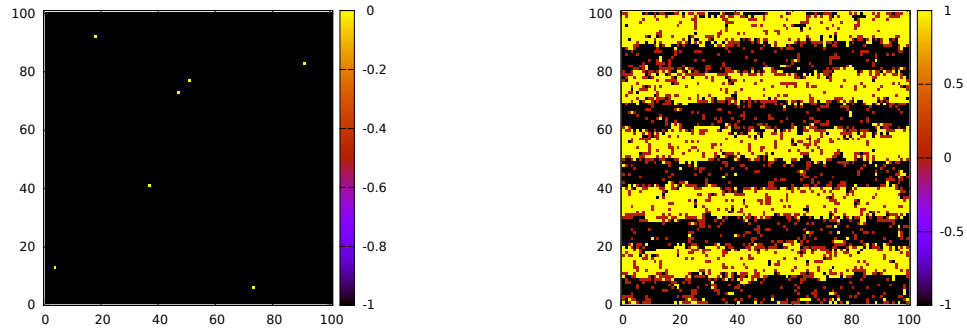


Figure 3.6: Morphologies of ordered or pinned (**left** for $H = 0.5$, $D = 0.5$ and $T = 0.5$) and disordered or standing spin-wave (**right** for $H = 1.5$, $D = 0.5$ and $T = 1.5$) phases. Here, $\lambda = 20$ $lu$.

signature of propagation of alternate spin-bands as observed in the case of propagating wave (see *figure 3.1* for comparison). It may again be worth mentioning here that these spin waves are not those conventional spin waves formed in solid state magnetic materials.

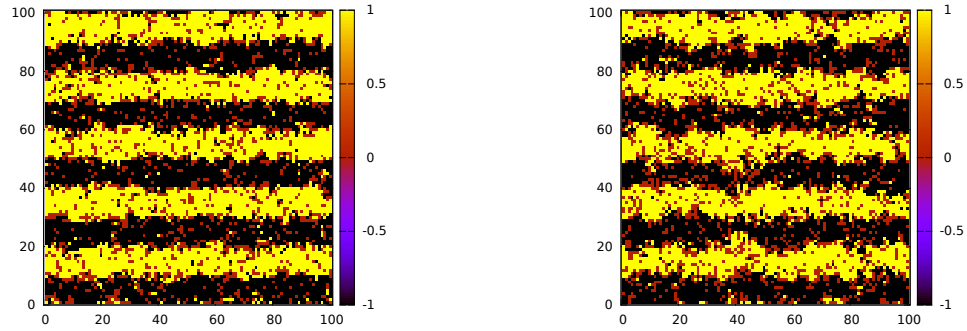


Figure 3.7: Morphologies of standing wave dynamical modes (non-propagating) in disordered phase for two different times. **Left** one is at $t = 1000$ MCSS and the **right** one is at $t = 1070$ MCSS. Here, $H = 1.5$, $T = 1.5$, $D = 0.5$ and $\lambda = 20$.

The dynamic phase transition is detected from the temperature ($T$) dependence of order parameter ($Q$) and variance of order parameter ($V$) for a fixed set of values of $h_0$ and $D$. Order parameter is defined as the time averaged magnetization per site over a full period of magnetic field oscillation. The value of order parameter is small (nearly zero) in high temperature, as the spins oscillate symmetrically with the magnetic field oscillation. It takes larger values when the temperature of the ferromagnet cools below the transition temperature $T_d$. Below $T_d$, thermal fluctuation and the external magnetic perturbation in the form of standing magnetic wave are not sufficient to break the mutual cooperative spin-spin interaction between the ferromagnetic spins and the spins are globally locked

in a parallel combination. This indicates the dynamical phase transition. *Figure 3.8* shows the typical variation of $Q$ with $T$ for four different set of values of $h_0$ ($H$ in figure) and $D$. The transition is detected from the peaks in the temperature variation of the variance $V$. The transition temperatures are found to depend on the values of $D$ and $h_0$.

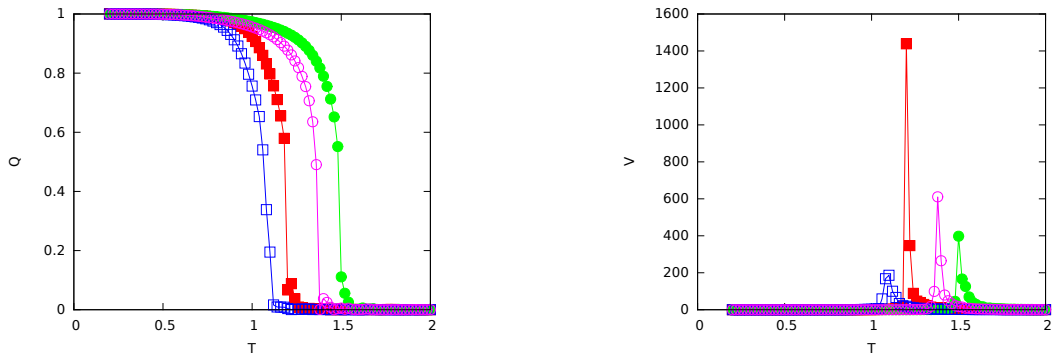


Figure 3.8: $Q$ and $V$ are plotted against temperature ($T$) for different values of field amplitude ($H$) and anisotropy ($D$) in the case of standing wave of wave length ($\lambda$) 20. Here, different symbols represent different values of $H$ and $D$. (i) Red filled square ($H = 1.0$, $D = 0.1$) (ii) Blue open square ($H = 1.0$, $D = 0.5$), (iii) Green filled circle ($H = 0.5$, $D = 0.1$) and (iv) Open magenta circle ($H = 0.5$, $D = 0.5$)

*Table 3.1* shows the comprehensive sample list of transition temperatures as obtained from the peak positions of $V$ in the *figure 3.8*.

Table 3.1: Dependence of transition temperature ($T$) on $h_0$ and $D$.

| $h_0$ | $D$ | $T_d$ |
|---|---|---|
| 0.50 | 0.10 | 1.50 |
| 0.50 | 0.50 | 1.38 |
| 1.00 | 0.10 | 1.20 |
| 1.00 | 0.50 | 1.10 |

Now, with various set of values of $h_0$, $D$ and $T_d$ phase boundaries may be drawn in the $h_0 - T$ plane for different values of $D$ and in the $D - T$ plane for different values of $h_0$. *Figure 3.9* shows the comprehensive phase boundaries. The nature of phase transition seems to be continuous through the entire range of phase boundaries. It is observed from the figure that the phase boundary in the $(h_0 - T)$ plane shrinks inward (lower values of $h_0$ ($H$ in figure) and $T$) as $D$ increases. Similarly, the phase boundary in the $D - T$ plane shrinks inward (lower values of $D$ and $T$) as $h_0$ ($H$ in figure) increases.

*Figure 3.10* shows a typical comparison of a phase diagram (for standing wave $D = 0.5$

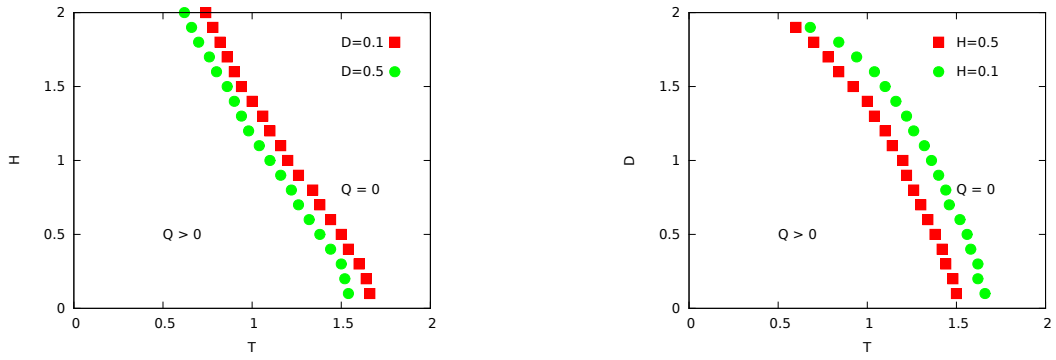


Figure 3.9: Phase diagram in the $H-T$ plane (**left**) and in the $D-T$ plane (**right**) in the case of standing wave. Different symbols denote different values of $D$ and $H$ (mentioned in the figure). Here $\lambda = 20$.

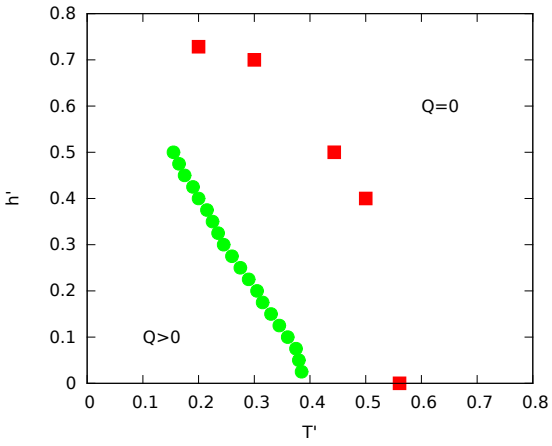


Figure 3.10: A typical comparison of phase diagrams. (i) (Red square) the Glauber kinetic $S = 1$ Blume-Capel model swept by oscillating (uniform over space) magnetic field in meanfield approximation. The data collected from *Fig-7(b)* of the reference [19] (ii) (Green bullet) The Monte Carlo metropolis results of $S = 1$ BC model swept by standing magnetic wave. $D = 0.5$ and $\lambda = 20$ here.

and $\lambda = 20$) of dynamic phase transition with that obtained from a meanfield study [19] of Glauber kinetic $S = 1$ BC model under uniformly oscillating magnetic field. The results, in this figure, are shown in a plot of suitably re-scaled temperature ($T' = T/z$) and field amplitude ($h' = h_0/z$). The variable $z$ represents the coordination number which is equal to 4 in the case of a square lattice (in this study).

The phase boundary corresponding to the MC study with standing magnetic wave like perturbation shrinks inward (lower values of $h'$ and $T'$) from that corresponding to the mean field study with uniformly oscillating magnetic field. This suggests that the spatio-temporal variation of the magnetic field decreases the transition temperature to a lower value as compared to that obtained from time varying field only.

## Bibliography:


1. M. Blume, Phys. Rev. **141** (1966) 517.
2. H. Capel, Physica. **32** (1966) 966.
3. M. Blume, V. J. Emery and R. B. Griffith, Phys. Rev. A **4** (1971) 1071.
4. D. M. Saul, M. Wortis and D. Stauffer, Phys. Rev. B. **9** (1974) 4964.
5. A. K. Jain and D. P. Landau, Phys. Rev. B, **22** (1980) 445.
6. M. Deserno, Phys. Rev. E, **56** (1997) 5204.
7. J. C. Xavier, F. C. Alcaraz, D. P. Lara, J. A. Plascak, Phys. Rev. E **57** (1998) 11575.
8. C. Yunus, B. Renklioglu, M. Keskin and A. N. Berker, Phys. Rev. E, **93** (2016) 062113.
9. J. A. Plascak, J. G. Moreira, F. C. saBarreto, Phys. Lett. A. **173** (1993) 360.
10. P. V. Santos, F. A. de Costa, J. M. de Araujo, Phys. Lett. A, **379** (2015) 1397.
11. Y. Yuksel, U. Akinci, H. Polat, Physica A **391** (2012) 2819.
12. E. V. Albano and K. Binder, Phys. Rev. E **85** (2012) 061601.
13. T. Fiig, B. M. Gorman, P. A. Rikvold and M. A. Novotny, Phys. Rev. E **50** (1994) 1930.
14. F. Manzo and E. Olivieri, J. Stat. Phys. **104** (2001) 1029.
15. C. Ekiz, M. Keskin and O. Yalcin, Physica A **293** (2001) 215.
16. M. Ertas, M. Keskin and B. Deviren, J. Magn. Magn. Mater. , **324** (2012) 1503.
17. E. Vatansever and H. Polat, J. Magn. Magn. Mater. , **332** (2013) 28.
18. M. Ertas, Y. Kokakaplan, M. Keskin, J. Magn. Magn. Mater. , **348** (2013) 113.
19. M. Keskin, O. Canko and U. Temizer, Phys. Rev. E, **72** (2005) 036125.
20. M. Acharyya, Acta Physica Polonica B, **45** (2014) 1027.
21. K. Binder and D. W. Heermann, Monte Carlo simulation in statistical physics, Springer series in solid state sciences, Springer, New-York, 1997.